

# 1 Global Sensitivity of Tropospheric Ozone to Precursor Emissions in

## 2 Clean and Present-Day Atmospheres: Insights from AerChemMIP

### 3 Simulations

4 Wei Wang<sup>1</sup> and Chloe Yuchao Gao<sup>2,3,\*</sup>

5 <sup>1</sup> Nanjing-Helsinki Institute in Atmospheric and Earth System Sciences, Nanjing  
6 University, Nanjing, 210023, China

7 <sup>2</sup> Department of Atmospheric and Oceanic Sciences & Shanghai Key Laboratory of  
8 Ocean-Land-Atmosphere Boundary Dynamics and Climate Change, Fudan  
9 University, Shanghai, 200438, China

10 <sup>3</sup> Institute of Eco-Chongming (IEC), Shanghai, 202151, China

11

12 \* Corresponding author: Chloe Yuchao Gao (gyc@fudan.edu.cn)

13 **Abstract**

14 Ozone ( $O_3$ ) is a Short-lived Climate Forcer (SLCF) that contributes to radiative  
15 forcing and indirectly affects the atmospheric lifetime of methane, a major  
16 greenhouse gas. This study investigates the sensitivity of global  $O_3$  to precursor  
17 gases in a clean atmosphere, where hydroxyl (OH) radical characteristics are more  
18 spatially uniform than in present-day conditions, using data from the *PiClim*  
19 experiments of the Aerosols and Chemistry Model Intercomparison Project  
20 (AerChemMIP) within the CMIP6 framework. We also evaluate the  $O_3$  simulation  
21 capabilities of four Earth system models (CESM2-WACCM, GFDL-ESM4, GISS-  
22 E2-1-G, and UKESM1-0-LL). Our analysis reveals that the CESM and GFDL  
23 models effectively capture seasonal  $O_3$  cycles and consistently simulate vertical  $O_3$   
24 distribution. While all models successfully simulate  $O_3$  responses to anthropogenic  
25 precursor emissions, CESM and GFDL show limited sensitivity to enhanced natural  
26  $NO_x$  emissions (e.g., from lightning) compared to GISS and UKESM. The  
27 sensitivities of  $O_3$  to its natural precursors ( $NO_x$  and VOCs) in GISS and UKESM  
28 models are substantially lower than their responses to anthropogenic emissions,  
29 particularly for lightning  $NO_x$  sources. These findings refine our understanding of  
30  $O_3$  sensitivity to natural precursors in clean atmospheres and provide insights for  
31 improving  $O_3$  predictions in Earth system models.

32 **1 Introduction**

33 Tropospheric ozone ( $O_3$ ) is a key air pollutant and atmospheric oxidant, exerting  
34 extensive influence on air quality and human health (Coffman et al., 2024; Lim et al.,  
35 2019; Malley et al., 2017; Nuvolone et al., 2018), climate systems, and  
36 biogeochemical processes (Hu et al., 2023; Fowler et al., 2009). As a Short-lived  
37 Climate Forcer (SLCF), tropospheric  $O_3$  exerts a radiative forcing of 0.35–0.5  $W\ m^{-2}$   
38 and influences atmospheric processes such as evaporation, cloud formation, and  
39 general circulation (Khomsi et al., 2022; Möller and Mauersberger, 1992; Rogelj et  
40 al., 2014; Stevenson et al., 2013). Furthermore,  $O_3$  plays a crucial role in regulating  
41 the terrestrial carbon sink and enhancing the formation of the hydroxyl (OH) radical  
42 (Naik et al., 2013b), which, in turn, affect the lifetime of methane (and halocarbons),  
43 the second most prominent anthropogenic greenhouse gas after carbon dioxide  
44 (KumAŞ et al., 2023).  $O_3$  also contributes to an increased atmospheric oxidation  
45 capacity, influencing the formation of secondary aerosols, such as organic aerosol,  
46 sulfate, and nitrate, which have significant implications for radiative forcing (Karsel  
47 et al., 2018).

48 While stratospheric  $O_3$  entrainment contributes to tropospheric  $O_3$  levels, the  
49 primary source of tropospheric  $O_3$  is photochemical production. This secondary  
50 pollutant is formed through photochemical oxidation reactions involving oxides of  
51 nitrogen ( $NO + NO_2 = NO_x$ ) and volatile organic compounds (VOCs) in the presence  
52 of OH and hydroperoxyl ( $HO_2$ ) radicals (Monks et al., 2015). The relationship  
53 between  $O_3$  and its precursors is nonlinear, making it challenging to mitigate  $O_3$   
54 pollution through simple precursor reduction strategies. Regional-scale sensitivity to  
55  $O_3$  precursors has been extensively investigated, such as emphasizing the diagnostic  
56 utility of ratios including  $O_3/NO_x$  (Jin et al., 2023; Sillman and He, 2002) and  
57  $VOC/NO_x$  (Li et al., 2024) for assessing  $O_3$ - $NO_x$ -VOC sensitivity, and nations such  
58 as the United Kingdom and the United States have demonstrated significant success  
59 in controlling regional ozone levels by implementing measures to reduce  $NO_x$   
60 emissions (Hakim et al., 2019). However, the global-scale sensitivity of  $O_3$  to its  
61 precursors has received limited attention, despite evidence suggesting that global  $O_3$   
62 forcing may have a more substantial impact on climate forcing than localized  $O_3$   
63 enhancements. Consequently, improving our understanding of  $O_3$  formation

64 mechanisms on a global scale is essential for effective air quality management and  
65 climate change mitigation strategies (Yu et al., 2021).

66 Recent studies utilizing Coupled Model Intercomparison Project Phase 6  
67 (CMIP6; Eyring et al., 2016) datasets have offered insights into the spatio-temporal  
68 evolution of the global tropospheric O<sub>3</sub> budget from 1850 to 2100 (Griffiths et al.,  
69 2021; Turnock et al., 2019) and have quantified the global stratosphere-troposphere  
70 O<sub>3</sub> exchange process (Li et al., 2024; Griffiths et al., 2021). However, challenges  
71 persist in quantifying the sensitivity of global O<sub>3</sub> to its precursors when assessing the  
72 increasing global O<sub>3</sub> forcing attributed to these precursors. These challenges arise  
73 from regional variability in meteorological conditions (Carrillo-Torres et al., 2017),  
74 differences in NO<sub>x</sub> and VOC volume mixing ratios (Jin et al., 2023; Sillman and He,  
75 2002), and the distinct characteristics of [hydroxyl radical](#) (OH) and [hydroperoxy](#)  
76 [radical](#) (HO<sub>2</sub>) influenced by varying degrees of urbanization (Karl et al., 2023;  
77 Vermeuel et al., 2019). Furthermore, while the observed upward trends in O<sub>3</sub> levels  
78 are primarily attributed to increased precursor emissions, limited research has  
79 investigated whether contemporary atmospheric conditions—shaped by climate  
80 warming and enhanced oxidation capacities—may be creating a more favorable  
81 environment for O<sub>3</sub> formation.

82 To address these gaps, this study investigates the sensitivity of global-scale O<sub>3</sub>  
83 to its precursors under a pre-industrial background atmosphere, with approximate  
84 [unified](#)[uniform](#) HO<sub>x</sub> conditions in major continental areas. We also examine the  
85 feedback mechanisms of different model responses to precursors from both  
86 anthropogenic and natural sources, using *PiClim* experiment data from the Aerosols  
87 and Chemistry Model Intercomparison Project (AerChemMIP) simulations (Collins  
88 et al., 2017) within CMIP6. Additionally, this research evaluates the ozone formation  
89 potential in the pre-industrial era based on contemporary (2014) emissions of O<sub>3</sub>  
90 precursors, with the aim of elucidating whether shifts in the background atmosphere  
91 have rendered it chemically more conducive to O<sub>3</sub> generation. Our analysis employs  
92 four models with interactive stratospheric and tropospheric chemistry, which have  
93 been extensively utilized in O<sub>3</sub>-related research (Brown et al., 2022; Griffiths et al.,  
94 2021; Tilmes et al., 2022; Zeng et al., 2022). This approach allows us to assess the  
95 global-scale sensitivity of O<sub>3</sub> to its precursors, evaluate the consistency and  
96 discrepancies among different models in representing O<sub>3</sub>-precursor relationships, and

97 provide insights into the potential impacts of changing emissions on future global O<sub>3</sub>  
98 levels and associated climate forcing, contributing to more accurate projections of  
99 future climate change.

100 **2 Models and methods**

101 **2.1 Model descriptions**

102 We use monthly-mean simulation data from four Earth system models in this  
103 study. The four chosen models possess the benefit of extensive applicability and a  
104 comprehensive *PiClim* ~~experimental-computational~~ framework. Table 1 summarizes  
105 key model features, including model resolution, vertical stratification, complexity of  
106 gas-phase chemistry, and relevant references. All models include interactive coupling  
107 of tropospheric and stratospheric chemistry with O<sub>3</sub> dynamics integrated into the  
108 radiation scheme, simulating the interaction between O<sub>3</sub> concentration and  
109 temperature. The response of simulated reactive gas emissions to chemical  
110 complexity is important. For example, changes in Biogenic Volatile Organic  
111 Compounds (BVOCs) can impact O<sub>3</sub>, methane lifetime, and potentially the oxidation  
112 of other aerosol precursors in models with interactive tropospheric chemistry [via OH](#)  
113 [changes](#).

**Table 1.** Information on model resolution, vertical levels, property of gas-phase chemistry and references.

Model	Resolution (lat × lon)	Number of gridpoints	Vertical levels	Aerosol model	Simulation reference
CESM2-WACCM	$192 \times 288$	55296	70 levels; top level $6 \times 10^{-6}$ hPa	MAM4	(Gettelman et al., 2019)
GFDL-ESM4	$180 \times 288$	51840	49 levels; top level 0.01 hPa	MATRIX	(Dunne et al., 2020; Horowitz et al., 2020)
GISS-E2-1-G	$90 \times 144$	12960	40 levels; top level 0.1 hPa	OMA	(Miller et al., 2014; Kelley et al., 2020)
UKESM1-0-LL	$144 \times 192$	27648	85 levels; top level 1 hPa	GLOMAP	(Mulcahy et al., 2018; Sellar et al., 2019)

116 CESM2-WACCM (hereafter “CESM”) is a fully coupled Earth system model  
117 that integrates the Community Earth System Model version 2 (Emmons et al., 2020)  
118 with the Whole Atmosphere Community Climate Model version 6 (WACCM6). The  
119 atmospheric component operates at a horizontal resolution of  $0.9375^{\circ}$  latitude by  $1.25^{\circ}$   
120 longitude, with 70 hybrid sigma-pressure vertical layers extending from the surface  
121 to  $6 \times 10^{-6}$  hPa. Its interactive chemistry and aerosol modules include the troposphere,  
122 stratosphere, and lower thermosphere, with a comprehensive treatment of 231 species,  
123 150 photolysis reactions, 403 gas-phase reactions, 13 tropospheric heterogeneous  
124 reactions, and 17 stratospheric heterogeneous reactions (Emmons et al., 2020). The  
125 model utilizes the four-mode Modal Aerosol Model (MAM4) (Emmons et al., 2020)  
126 and features its secondary organic aerosol (SOA) framework based on the Volatility  
127 Basis Set (VBS, Donahue et al., 2013) approach. The photolytic calculations use both  
128 inline chemical modules and a lookup table approach, which does not consider  
129 changes in aerosols.

130 The Atmospheric Model version 4.1 (AM4.1, Horowitz et al. (2020)) within the  
131 GFDL Earth system model (Dunne et al., 2020) incorporates an interactive chemistry  
132 scheme that spans both the troposphere and stratosphere (GFDL-ESM4; hereafter  
133 “GFDL”). The atmospheric component operates at a horizontal resolution of  $1^{\circ}$   
134 latitude by  $1.25^{\circ}$  longitude, with 49 hybrid sigma-pressure vertical layers extending  
135 from the surface to 0.01 hPa. This scheme includes 56 prognostic tracers, 36  
136 diagnostic species, 43 photolysis reactions, 190 gas-phase kinetic reactions, and 15  
137 heterogeneous reactions. Stratospheric chemistry accounts for key  $O_3$  depletion  
138 cycles ( $O_x$ ,  $HO_x$ ,  $NO_x$ ,  $ClO_x$ , and  $BrO_x$ ) and heterogeneous reactions on stratospheric  
139 aerosols (Austin et al., 2013). Photolysis rates are calculated dynamically with the  
140 FAST-JX version 7.1 code, which considers the radiative impacts of modeled  
141 aerosols and clouds. The chemical mechanism is further elaborated in Horowitz et al.  
142 (2020), and the gas-phase and heterogeneous chemistry are similar to those employed  
143 by Schnell et al. (2018). Non-interactive natural emissions of  $O_3$  precursors are  
144 prescribed as outlined in Naik et al. (2013a).

145 The GISS model, developed by the NASA Goddard Institute for Space Studies,  
146 integrates the chemistry-climate model version E2.1 with the GISS Ocean v1 (G01)  
147 model (GISS-E2-1-G; hereafter “GISS”). The specific configurations of this model

148 utilized for the CMIP6 are detailed in Kelley et al. (2020). In this study, we focus on  
149 the model subset that includes online interactive chemistry. The atmospheric  
150 component operates at a horizontal resolution of  $2^{\circ}$  latitude by  $2.5^{\circ}$  longitude, with  
151 40 hybrid sigma-pressure vertical layers extending from the surface to 0.1 hPa. The  
152 interactive chemistry module employs the GISS Physical Understanding of  
153 Composition-Climate Interactions and Impacts (G-PUCCINI) mechanism for gas-  
154 phase chemistry (Kelley et al., 2020; Shindell et al., 2013). For aerosols, the model  
155 utilizes either the One-Moment Aerosol (OMA) or the Multiconfiguration Aerosol  
156 Tracker of Mixing state (MATRIX) model (Bauer et al., 2020). The gas-phase  
157 chemistry involves 146 reactions, including 28 photodissociation reactions, affecting  
158 47 species across the troposphere and stratosphere, along with an additional five  
159 heterogeneous reactions. The model transports 26 aerosol particle tracers and 34 gas-  
160 phase tracers (OMA).

161 UKESM represents the United Kingdom's Earth system model (Sellar et al.,  
162 2019). It builds upon the Global Coupled 3.1 (GC3.1) configuration of HadGEM3  
163 (Williams et al., 2018), incorporating additional Earth system components, such as  
164 ocean biogeochemistry, the terrestrial carbon-nitrogen cycle, and atmospheric  
165 chemistry (UKESM1-0-LL; hereafter "UKESM"). Walters et al. (2019) provided  
166 descriptions of the atmospheric and land components. The atmospheric component  
167 operates at a horizontal resolution of  $1.25^{\circ}$  latitude by  $1.875^{\circ}$  longitude, with 85  
168 vertical layers extending from the surface to 85 km. The chemistry module in the  
169 UKESM model is a unified stratosphere-troposphere scheme (Archibald et al., 2020)  
170 including 84 tracers, 199 bimolecular reactions, 25 unimolecular and termolecular  
171 reactions, 59 photolytic reactions, 5 heterogeneous reactions, and 3 aqueous-phase  
172 reactions for the sulfur cycle from the United Kingdom Chemistry and Aerosols  
173 (UKCA) model. The aerosol module is based on the two-moment scheme from  
174 UKCA, known as GLOMAP mode, and is integrated into the Global Atmosphere  
175 7.0/7.1 configuration of HadGEM3 (Walters et al., 2019). The UKESM uses  
176 interactive Fast-JX photolysis scheme, which is applied to derive photolysis rates  
177 between 177 and 850 nm, as described in Telford et al. (2013). In the lower  
178 mesosphere, photolysis rates are calculated using lookup tables (Lary and Pyle, 1991).

179 Models differ in their representation of O<sub>3</sub> source and sink processes, as well as  
180 in the definitions of the associated budget terms, which contributes to variability in

181 model outcomes (Stevenson et al., 2006; Young et al., 2018). For example, in the  
182 GISS model, the tropospheric chemistry component simulates the  $\text{NO}_x\text{-HO}_x\text{-O}_x\text{-CO}$ -  
183  $\text{CH}_4$  system and the oxidation pathways for non-methane volatile organic compounds  
184 (NMVOCs). Central to these discrepancies are the treatments of non-methane volatile  
185 organic compound NMVOCs chemistry, which impacts both chemical production  
186 and destruction rates, along with surface removal mechanisms and stratospheric  
187 influences. Furthermore, the choice of tropopause definition can significantly alter  
188 the diagnosed  $\text{O}_3$  burden, as well as the flux from the stratosphere.

189 All four of the interactive tropospheric chemistry models contain  
190 parameterizations of the nitrogen oxide ( $\text{NO}_x$ ) emissions from lightning based on the  
191 height of the convective cloud top (Price et al., 1997; Price and Rind, 1992; Price,  
192 2013), and the tropopause height for each model based on the WMO definition. Each  
193 model has a different way of implementing emissions and how much they are profiled.  
194 For instance, online calculations of lightning  $\text{NO}_x$  emissions during deep convection  
195 in the GISS model are based on the method described by (Kelley et al., 2020).  
196 Lightning  $\text{NO}_x$  continues to be a major source of uncertainty in both model  
197 comparisons and the temporal development of tropospheric  $\text{O}_3$  because it has a  
198 disproportionately significant influence on tropospheric- $\text{O}_3$  concentration relative to  
199 surface emissions (Murray et al., 2013).

200 BVOC emissions are modeled as a function of vegetation type and cover, as well  
201 as temperature and photosynthetic rates (gross primary productivity) (Unger, 2014;  
202 Sporre et al., 2019; Pacifico et al., 2011; Guenther et al., 1995). While models vary  
203 in the speciation of emitted VOCs, they commonly include isoprene and  
204 monoterpenes, each with its own distinct emission parameterization. Despite the  
205 common reliance on photosynthetically active radiation for the parameterization of  
206 BVOC emissions across the four models, there exist notable distinctions. For instance,  
207 the GFDL model exclusively considers the leaf area index, neglecting the impact of  
208 temperature on BVOC emissions, and the CESM, GISS, and UKESM models omit  
209 the influence of vegetation type from their calculations.

## 210 **2.2 Simulation data and experimental design**

211 The primary objective of AerChemMIP is to quantitatively ascertain the  
212 influence of aerosols and reactive trace gases on the climate system, as well as the

213 bidirectional feedback mechanisms involved (Collins et al., 2017). Table 2 presents  
214 a synopsis of the experimental configurations employed in this study. The control  
215 experiment, denoted as *PiClim-control*, is designed to stabilize both atmospheric  
216 composition and climatic conditions at a state reminiscent of the pre-industrial era,  
217 where the natural fractions of stratospheric ozone forcing species such as halocarbons  
218 was extremely low, specifically 1850. The *PiClim-2x* experiment involves doubling  
219 of individual natural emission fluxes relative to the 1850 control, while the *PiClim-x*  
220 experiments calibrate these fluxes to align with the emission levels prevalent in 2014  
221 (Collins et al., 2017). *PiClim-2xNO<sub>x</sub>* represents to doubling of the nitric oxide  
222 emissions from natural sources due to lightning activity doubles. *PiClim-2xVOC*  
223 represents to doubling of the volatile organic compound emissions from natural  
224 sources, including isoprene and monoterpenes, doubles. *PiClim-HC* represents the  
225 pre-industrial climatological control with 2014 halocarbons emissions both from  
226 anthropogenic (CFCs, HCFCs and compounds containing bromine) and natural  
227 sources. *PiClim-CH<sub>4</sub>* represents the pre-industrial climatological control with 2014  
228 methane emissions both from anthropogenic and natural sources. *PiClim-NO<sub>x</sub>*  
229 represents the pre-industrial climatological control with 2014 nitrogen oxide  
230 emissions both from anthropogenic and natural sources. *PiClim-VOC* represents the  
231 pre-industrial climatological control with 2014 VOC emissions both from  
232 anthropogenic and natural sources. *PiClim-NTCF* represents the pre-industrial  
233 climatological control with 2014 near-term climate forcers emissions, including  
234 aerosols and chemically reactive gases such as tropospheric ozone and methane.  
235 *PiClim-N<sub>2</sub>O* represents the pre-industrial climatological control with 2014 nitrous  
236 oxide emissions both from anthropogenic and natural sources. *PiClim-aer* represents  
237 the pre-industrial climatological control with 2014 aerosol concentrations. *PiClim-*  
238 *O<sub>3</sub>* represents the pre-industrial climatological control with 2014 ozone  
239 concentrations. *HC* represents halocarbons include CFCs, HCFCs and compounds  
240 containing bromine. *NTCF* represents near-term climate forcers, including aerosols  
241 and chemically reactive gases such as tropospheric ozone and methane. *PiClim-BC*  
242 represents the pre-industrial climatological control with 2014 black carbon  
243 concentrations. *PiClim-BC* represents black carbon and *N<sub>2</sub>O* represents nitrous oxide.

244

**Table 2.** The available experiments of selected models in this study. "X" represents the experiment is available

Model	<i>PiClim-</i>											
	<i>2xNO<sub>x</sub></i>	<i>2xVOC</i>	<i>HC</i>	<i>CH<sub>4</sub></i>	<i>NO<sub>x</sub></i>	<i>VOC</i>	<i>NTCF</i>	<i>N<sub>2</sub>O</i>	<i>O<sub>3</sub></i>	<i>aer</i>	<i>control</i>	<i>BC</i>
CESM2-WACCM	X	X	X	X	X	X	X	X	X			
GFDL-ESM4	X	X	X		X	X			X	X	X	X
GISS-E2-1-G	X	X	X	X	X	X	X	X	X	X	X	X
UKESM1-0-LL	X	X	X	X	X	X	X	X	X	X	X	X

245

246 We analyzed models that had archived sufficient data in the Earth System Grid  
247 Federation (ESGF) system to permit accurate characterization of tropospheric O<sub>3</sub>. In  
248 practice this meant we used archived O<sub>3</sub> data from the AERmon characterization of  
249 the tropospheric O<sub>3</sub> (variable name: “o3”) on native model grids. Other variables used  
250 include chemical production (variable name: “o3prod”), chemical destruction  
251 (variable name: “o3loss”), nitrogen monoxide (variable name: “no”), nitrogen  
252 dioxide (variable name: “no2”), isoprene (variable name: “isop”), organic dry aerosol  
253 (variable name: “emioa”), and secondary organic aerosol (variable name: “mmrsoa”).  
254 All data used in this paper are available on the Earth System Grid Federation website  
255 and can be downloaded from <https://esgf-index1.ceda.ac.uk/search/cmip6-ceda/> (last  
256 access: 4 July 2024, ESGF-CEDA, 2020).

257 A new set of historical anthropogenic emissions has been developed with the  
258 Community Emissions Data System (CEDS, Hoesly et al., 2018). CEDS uses updated  
259 emission factors to provide monthly emissions of the major aerosol and trace gas  
260 species over the period 1750 to 2014 for use in CMIP6, and biomass burning  
261 emissions are based on a different inventory developed separate from CEDS (Van  
262 Marle et al., 2017). The primary analysis examines emissions of NO<sub>x</sub> and VOCs from  
263 anthropogenic (Hoesly et al., 2018) and biomass burning sources (van Marle et al.,  
264 2017) that were provided as a common emission inventory to be used by all models  
265 (including the four in this study) in CMIP6 simulations. In the CESM and GFDL  
266 models, biogenic emissions, including isoprene and monoterpenes, are calculated  
267 interactively using MEGAN version 2.1 (Guenther et al., 2012) and are further  
268 utilized for SOA formation. While in the GISS model, biogenic emissions of isoprene  
269 are computed online and are sensitive to temperature (Shindell et al., 2006), whereas  
270 alkenes, paraffins, and terpenes are prescribed. And in the UKESM model, emissions  
271 of isoprene and monoterpenes are interactively calculated using the iBVOC emission  
272 model (Pacifico et al., 2011).

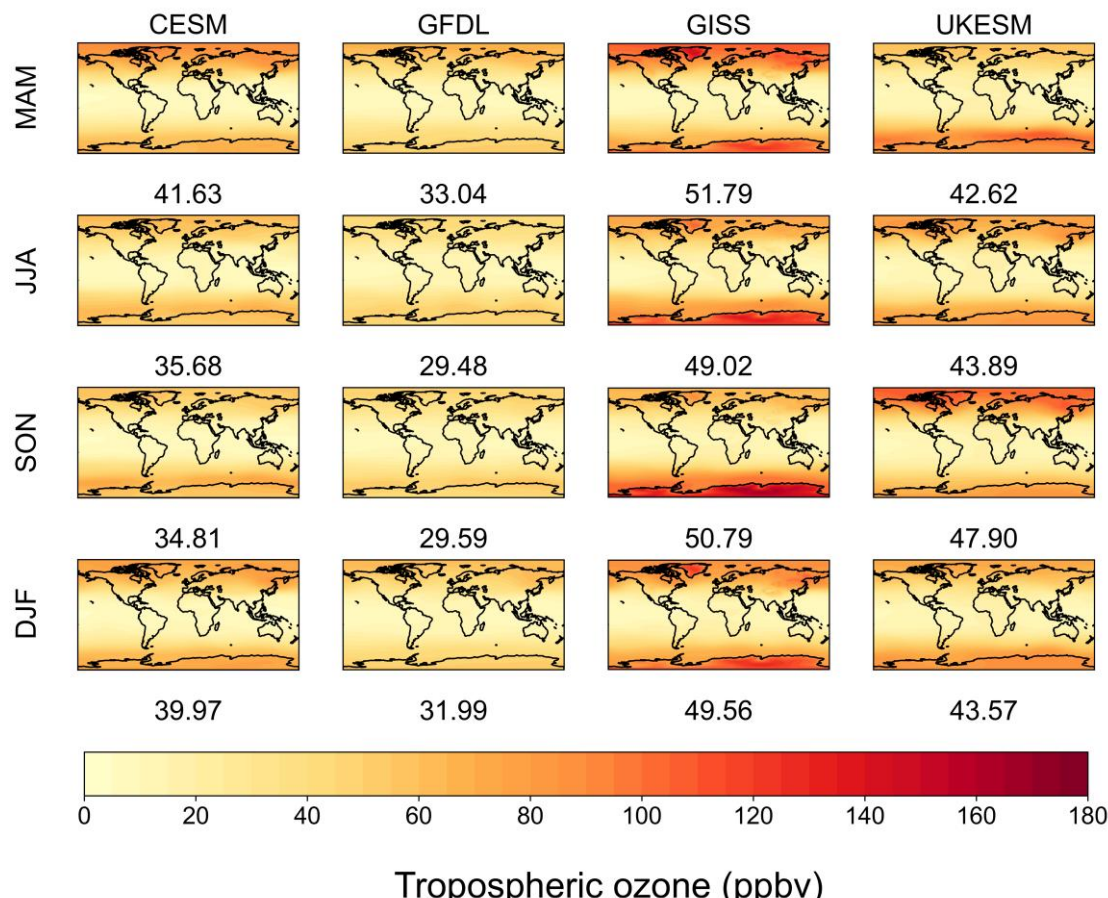
### 273 **3 Results and Discussions**

#### 274 **3.1 Spatial, seasonal, and vertical distribution of tropospheric O<sub>3</sub>**

275 We first investigate the seasonal and vertical variations of ozone volume mixing  
276 ratio in the pre-industrial atmospheres simulated by four selected models. The  
277 analysis of tropospheric O<sub>3</sub> data derived from the *PiClim* experiment outcomes of

278 CMIP6 models reveals distinct seasonal cycles and inter-model variations (Fig. 1).  
 279 The GISS model demonstrates the highest simulated tropospheric column O<sub>3</sub> volume  
 280 mixing ratio at 50.29 ppbv in the 29<sup>th</sup> and 30<sup>th</sup> year of simulation, followed by the  
 281 UKESM (44.50 ppbv), CESM (38.02 ppbv), and GFDL (31.03 ppbv), where the  
 282 height of the tropopause is based on the definition of WMO. These are consistent with  
 283 previous findings from historical experiments (Griffiths et al., 2021).

284 Furthermore, our analysis indicates that the disparity in O<sub>3</sub> volume mixing ratio  
 285 during the *PiClim* experiment primarily occurs in polar regions. This may be  
 286 attributed to the GISS model's ability to replicate a more robust entrainment of  
 287 stratospheric O<sub>3</sub>, a key source of tropospheric O<sub>3</sub> in the pre-industrial atmosphere,  
 288 particularly at the poles. Previous studies have demonstrated that elevated O<sub>3</sub> levels  
 289 in the Arctic during MAM and DJF, as well as in the Antarctic during JJA and SON,  
 290 result from the cumulative impact of the polar O<sub>3</sub> barrier (Romanowsky et al., 2019).



291  
 292 **Figure 1.** Comparison of the seasonal cycle of tropospheric column averaged volume  
 293 mixing ratio of O<sub>3</sub> ([density weighted](#)) of the *PiClim* experiment results in the 29<sup>th</sup> and  
 294 30<sup>th</sup> year of simulation of the four models. Each row shows a separate meteorological  
 295 season, arranged from top to bottom: March to May (MAM), June to August (JJA),

296 September to November (SON), and December to February (DJF). Each column  
297 represents a selected model, listed from left to right: CESM, GFDL, GISS, and  
298 UKESM. The figures displayed below each chart represent the global average ozone  
299 volume mixing ratio.

300 Seasonal variations in tropospheric O<sub>3</sub> volume mixing ratio exhibit model-  
301 specific patterns. The CESM, GFDL, and GISS models simulate peak tropospheric  
302 O<sub>3</sub> volume mixing ratio in spring during the *PiClim* experiments. In contrast, the  
303 UKESM model reproduces maximum O<sub>3</sub> volume mixing ratio in autumn, indicating  
304 a limited capability in simulating dynamic circulations in the tropopause.  
305 Furthermore, the seasonal O<sub>3</sub> cycle simulations in CESM, GFDL, and GISS exhibit  
306 distinct discrepancies in their outcomes. For instance, the CESM model simulates the  
307 lowest O<sub>3</sub> volume mixing ratio in SON, while the GFDL model exhibits the lowest  
308 volume mixing ratio in JJA. The GISS model simulation indicates higher O<sub>3</sub> levels in  
309 autumn compared to DJF, which is consistent with results from historical experiments  
310 (Griffiths et al., 2021). Additionally, our analysis reveals that the CESM simulations  
311 demonstrate the most pronounced seasonal oscillation amplitude in O<sub>3</sub> volume  
312 mixing ratio, approximately 6.82 ppbv. This feature underscores the model's  
313 sensitivity to seasonal factors affecting tropospheric O<sub>3</sub> dynamics.

314 In the *PiClim* experiments, all four models accurately reproduce the peak volume  
315 mixing ratio of O<sub>3</sub> in the middle stratosphere at 10 hPa and the zonal average mixing  
316 ratios reaching their peak in the upper troposphere, particularly in extratropical  
317 regions, indicative of extended chemical lifetimes at higher altitudes. However,  
318 notable disparities are observed in the vertical distribution characteristics of O<sub>3</sub>  
319 among the four models (Fig. 2). Specifically, the CESM model exhibits the highest  
320 vertical extension, including an additional hotspot simulated in the thermosphere.  
321 While the GFDL and CESM2 models exhibit consistent simulation outcomes below  
322 0.01 hPa, GISS and UKESM simulate significantly higher stratospheric O<sub>3</sub> levels at  
323 10 hPa in comparison.

324 Notable distinctions are observed in the spatial distribution of O<sub>3</sub>. The GISS  
325 model simulates a more vertically concentrated and latitudinally extended O<sub>3</sub>  
326 distribution. This characteristic may be a crucial factor contributing to the pronounced  
327 impact of O<sub>3</sub> transport in the polar stratosphere, as simulated by GISS. The zonal  
328 variability in O<sub>3</sub> distribution simulated by the UKESM falls between that of the GISS  
329 and CESM models. These inter-model discrepancies in O<sub>3</sub> simulation results likely

reflect suboptimal representation of local and regional dynamics, as well as omitted chemical processes in corresponding models. The variability and uncertainty in O<sub>3</sub> precursor emission estimates further exacerbate these disparities.

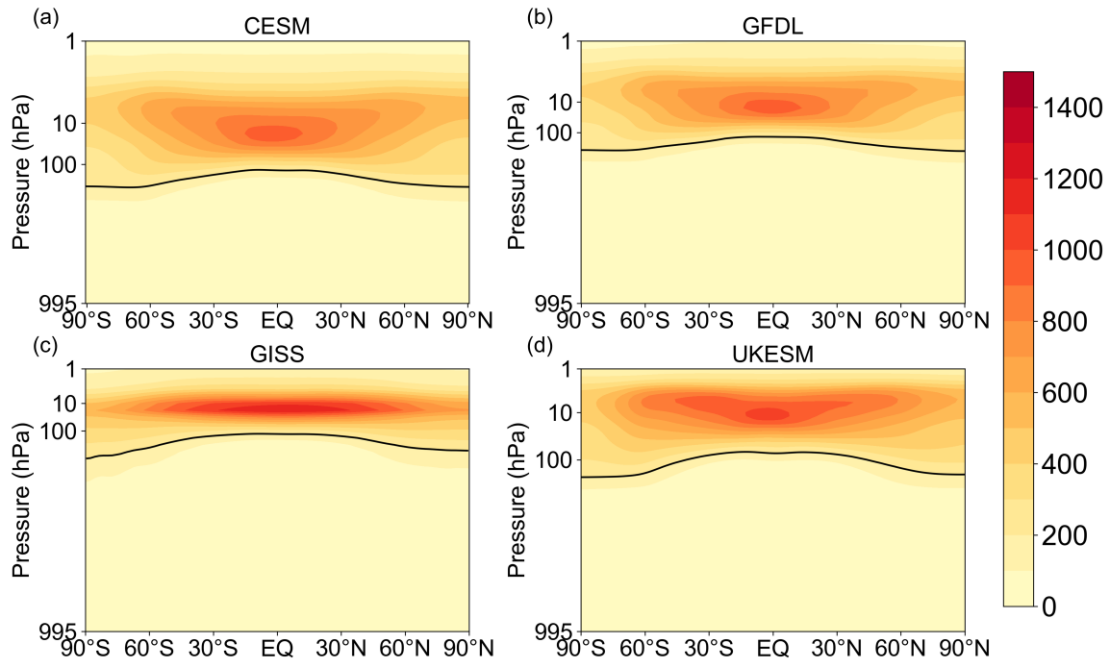


**Figure 2.** The zonal mean O<sub>3</sub> distribution for the 29<sup>th</sup> and 30<sup>th</sup> year of the *PiClim* experiment results from the (a) CESM, (b) GFDL, (c) GISS, and (d) UKESM model. Thick black lines represent the tropopause height for each model based on the WMO definition.

### 3.2 Characteristics of tropospheric O<sub>3</sub> under various experiments

Tables 3 and 4 present the global O<sub>3</sub> volume mixing ratio and tropospheric O<sub>3</sub> volume mixing ratio across all experiments from the four different models. The GISS model simulations show higher tropospheric O<sub>3</sub> volume mixing ratios, reflecting increased rates of stratospheric downwelling and surface O<sub>3</sub> precursor emissions. However, its overall O<sub>3</sub> volume mixing ratio is notably lower compared to the UKESM, CESM, and GFDL models, with reductions of 114.24, 76.16, and 47.04 ppbv, respectively. Analysis reveals that in the CESM, GFDL, and GISS models, the global O<sub>3</sub> molar fraction in the *PiClim-2NO<sub>x</sub>* and *PiClim-NO<sub>x</sub>* experiments surpasses that in the *PiClim-2VOC* and *PiClim-VOC* experiments. This difference is most pronounced in the GISS model, aligning with previous findings indicating its heightened sensitivity to NO<sub>x</sub> response (Turnock et al., 2019). Conversely, in the UKESM model, the global O<sub>3</sub> molar fraction of the *PiClim-2NO<sub>x</sub>* experiment is lower than that of the *PiClim-2VOC* experiment. Interestingly, the tropospheric O<sub>3</sub> volume mixing ratios in the *PiClim-2NO<sub>x</sub>* experiment in the CESM and GFDL models

353 are notably lower than in their respective *PiClim-2VOC* experiments, with reductions  
354 of 0.41 and 0.29 ppbv. This discrepancy challenges the conventional understanding  
355 that increased NO<sub>x</sub> emissions from lightning activity should lead to tropospheric O<sub>3</sub>  
356 generation, suggesting a need for enhanced sensitivity simulations in these two  
357 models regarding O<sub>3</sub> and NO<sub>x</sub> emissions from natural sources due to lightning activity.  
358 In contrast, the *PiClim-2NO<sub>x</sub>* experiments of the GISS and UKESM models  
359 effectively simulate an increase in tropospheric O<sub>3</sub> volume mixing ratio compared to  
360 their *PiClim-2VOC* experiments. Furthermore, across all four models, the  
361 tropospheric O<sub>3</sub> volume mixing ratio of the *PiClim-NO<sub>x</sub>* experiment surpasses that of  
362 the *PiClim-VOC* experiment, indicating the models' ability to accurately replicate the  
363 impact of rising anthropogenic emissions on O<sub>3</sub> production. Additionally, methane, a  
364 crucial natural source of volatile organic compounds and a key greenhouse gas,  
365 enhances tropospheric O<sub>3</sub> generation by CH<sub>4</sub> oxidation and influencing temperature,  
366 thereby elevating global O<sub>3</sub> volume mixing ratio. This phenomenon contributes to the  
367 heightened sensitivity of O<sub>3</sub> to methane volume mixing ratio in a clean atmosphere.  
368 Elevated volume mixing ratios of HCFCs (*PiClim-HC*) and nitrous oxide~~methane~~  
369 (*PiClim-* N<sub>2</sub>OCH<sub>4</sub>) lead to substantial stratospheric O<sub>3</sub> depletion, consequently  
370 affecting tropospheric O<sub>3</sub> volume mixing ratio through the pod coil process. Other  
371 influencing factors, such as aerosols and black carbon, induce warming through  
372 radiation effects, thereby simulating elevated O<sub>3</sub> volume mixing ratio.

373  
374

**Table 3.** The averaged [volume mixing ratio](#) and [concentrations](#) of [global stratospheric ozone](#) and [global ozone](#) at all simulated vertical levels in the 29<sup>th</sup> and 30<sup>th</sup> year for each experiment of four models (ppbv).

Model	<i>PiClim-</i>											
	<i>2xNO<sub>x</sub></i>	<i>2xVOC</i>	<i>HC</i>	<i>CH<sub>4</sub></i>	<i>NO<sub>x</sub></i>	<i>VOC</i>	<i>NTCF</i>	<i>N<sub>2</sub>O</i>	<i>O<sub>3</sub></i>	<i>aer</i>	<i>control</i>	<i>BC</i>
CESM2-WACCM	726.06	725.95	662.71	713.80	728.61	727.06	725.42	710.94				
GFDL-ESM4	628.63	626.68	571.32		632.03	628.92			632.70	628.44	629.98	629.78
GISS-E2-1-G	490.91	482.13	422.65	493.27	490.22	480.93	486.46	471.84	485.17	486.54	484.76	484.82
UKESM1-0-LL	707.27	707.93	613.89	697.32	716.14	704.78	723.99	694.44	714.27	697.04	702.88	701.81

375

376

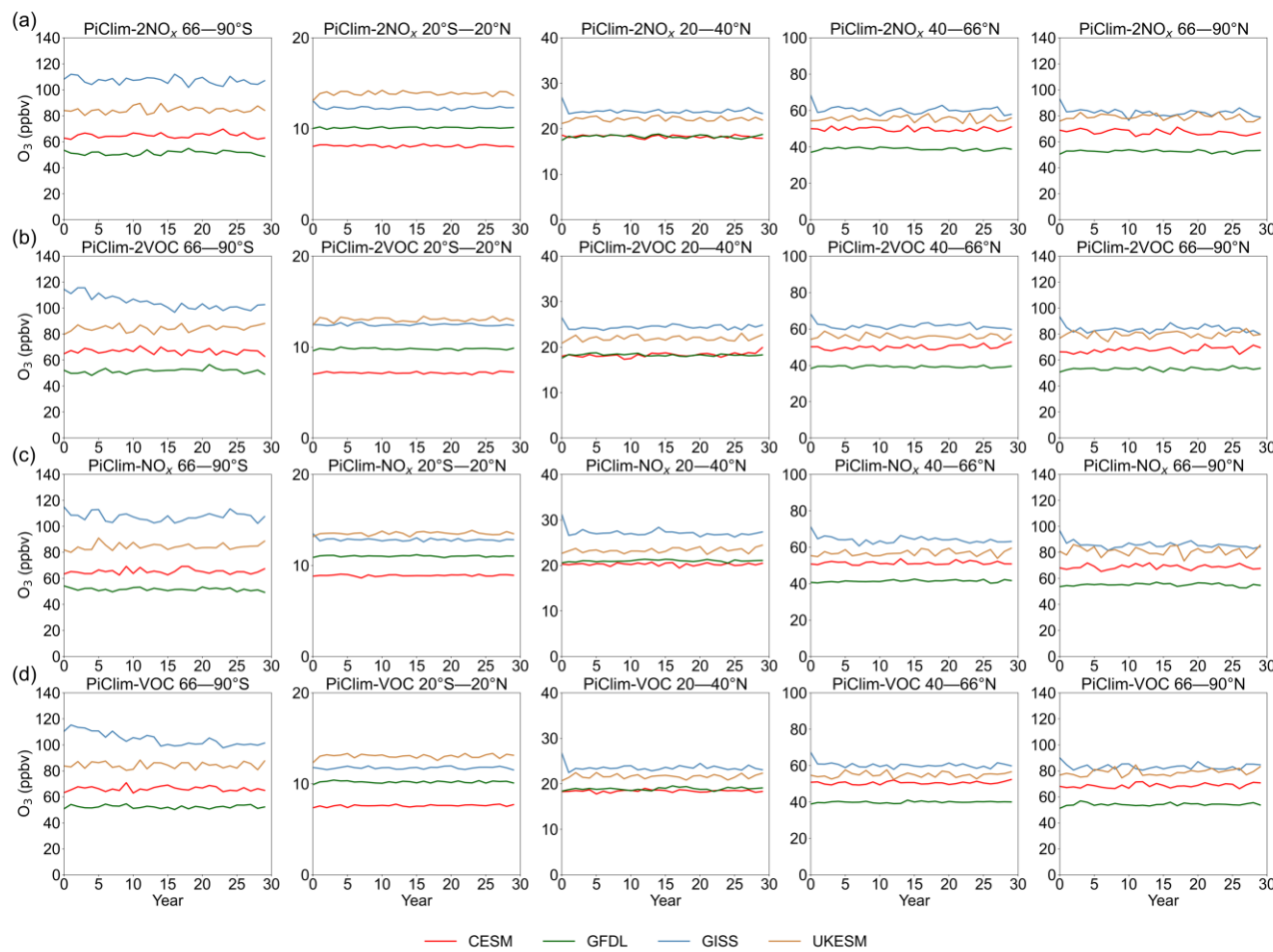
377

**Table 4.** The averaged [volume mixing ratio concentrations](#) of global tropospheric ozone in the 29<sup>th</sup> and 30<sup>th</sup> year for each experiment of four models (ppbv).

Model	<i>PiClim-</i>	2xNO <sub>x</sub>	2xVOC	HC	CH <sub>4</sub>	NO <sub>x</sub>	VOC	NTCF	N <sub>2</sub> O	O <sub>3</sub>	aer	control	BC
CESM2-WACCM		38.17	38.58	33.44	39.42	39.16	39.14	41.33	38.10				
GFDL-ESM4		31.33	31.62	24.42		32.64	32.25			34.09	31.01	30.79	30.95
GISS-E2-1-G		52.30	50.96	44.18	53.08	52.14	50.21	51.65	48.36	52.47	50.36	49.27	50.02
UKESM1-0-LL		47.53	46.14	31.04	45.55	46.02	45.97	47.29	45.04	46.65	43.69	46.70	45.11

378

379 Figure 3 shows the temporal evolution of tropospheric O<sub>3</sub> levels across various  
380 latitudes, as simulated by four distinct models in O<sub>3</sub> precursor experiments. In the  
381 *PiClim* experiments, none of the models predicted an enhancement in O<sub>3</sub> volume  
382 mixing ratio [with simulation time at all latitudes](#), reflecting the consistent chemical  
383 lifetime of O<sub>3</sub> within the pristine atmospheric conditions. However, discrepancies in  
384 O<sub>3</sub> predictions among the models become more pronounced with increasing latitudes.  
385 While the CESM model generally exhibits higher tropospheric O<sub>3</sub> volume mixing  
386 ratios compared to the GFDL model, it paradoxically portrays the lowest O<sub>3</sub> levels in  
387 the equatorial region. The GISS model demonstrates a marked disparity in  
388 tropospheric O<sub>3</sub> volume mixing ratios between the Antarctic and Arctic regions, with  
389 the former registering notably higher levels. In contrast, the CESM and GFDL models  
390 exhibit similar patterns in this regard. A unique feature of the GISS model is a notable  
391 declining trend in Antarctic tropospheric O<sub>3</sub> levels during the initial 15 years of both  
392 the *PiClim-2VOC* and *PiClim-VOC* experiments. This trend is not observed in the  
393 CESM, GFDL, and UKESM models, highlighting [a distinctive characteristic of the](#)  
394 [GISS model's simulation](#)[the sensitivity of the GISS model to precursors in simulating](#)  
395 [ozone is still higher than that of other models even in the pre-industrial clean](#)  
396 [atmosphere. The same conclusion was reached for NO<sub>x</sub> experiments, but the ozone](#)  
397 [forcing was less than that in the VOC experiments](#). The UKESM model stands out  
398 with its pronounced simulation of elevated O<sub>3</sub> volume mixing ratios in the tropical  
399 belt. Furthermore, the *PiClim-2xVOC* experiment conducted within the UKESM  
400 model demonstrates a significant O<sub>3</sub> response to enhanced emissions of VOCs from  
401 natural sources in the equatorial region. This suggests a strong sensitivity of O<sub>3</sub> in the  
402 UKESM to increases in VOC emissions from natural sources.



403

404 **Figure 3.** The temporal evolution characteristics of annual mean tropospheric column averaged O<sub>3</sub> volume mixing ratio at different latitudes for  
 405 each model are presented for the (a) *PiClim-2NO<sub>x</sub>*, (b) *PiClim-2VOC*, (c) *PiClim-NO<sub>x</sub>*, and (d) *PiClim-VOC* experiment, [the 4 models are](#)  
 406 [represented by different line colors](#).

407 **3.3 Analysis of O<sub>3</sub> generation in precursor experiments**

408 In the shown subset of *PiClim*In the *PiClim* experiments, the O<sub>3</sub> production was  
409 defined as the cumulative tendency from HO<sub>2</sub>, CH<sub>3</sub>O<sub>2</sub>, RO<sub>2</sub>, and NO reactions, while  
410 O<sub>3</sub> loss encompassed the sum of O(1D) + H<sub>2</sub>O, O<sub>3</sub> + HO<sub>2</sub>, OH + O<sub>3</sub>, and O<sub>3</sub> + alkene  
411 reactions. Figure 4 depicts the chemical production and consumption of tropospheric  
412 ozone in the five simulations performed by the4 four modelsdifferent experiments of  
413 the four models. The GISS demonstrates the lowest O<sub>3</sub> chemical production among  
414 the models, whereas the other three models show generally consistent production  
415 levels. Notably, the GISS model exhibits a relatively low efficiency in O<sub>3</sub> chemical  
416 consumptions, primarily due to missing the loss of O<sub>3</sub> with isoprene and terpenes  
417 process. The low offset of ozone production and depletion in the pre-industrial  
418 atmosphere by the GISS model provides a new perspective based on previous studies  
419 indicating the high offset of ozone production and depletion in the present atmosphere  
420 by the GISS model. The four models all showed high ozone chemical production in  
421 the *PiClim-NO<sub>x</sub>* experiment, indicating that the four all have perfect ability to  
422 simulate the photochemical generation mechanism of tropospheric ozone. However,  
423 the CESM and GFDL models do not show a significant increase in tropospheric O<sub>3</sub>  
424 chemical generation during the *PiClim-2NO<sub>x</sub>* experiment. And although the GISS and  
425 UKESM models successfully simulated an increase in the O<sub>3</sub> chemical generation  
426 rate due to heightened lightning activity in this experiment, these increases in ozone  
427 production are also much smaller than the chemical production generated by the  
428 *PiClim-NO<sub>x</sub>* experiment, which might show that the theoretical mechanism of ozone  
429 sensitivity to natural precursors in pre-industrial atmosphere differs from the present  
430 mechanism due to the differences in the characteristics of intermediate products such  
431 as OH. Furthermore, in either model, the ozone chemical production from the *PiClim-*  
432 *NO<sub>x</sub>* experiment, while higher than in other experiments other than *PiClim-NTCF*, is  
433 much smaller than the ozone chemical production caused by this emission inventory  
434 in the atmosphere today (Fig. S5). Today's NO<sub>x</sub> emission forcing has not led to a  
435 sustained increase in the ozone volume mixing ratio in the pre-industrial atmosphere  
436 over a long-time scale, which indicates important differences between the pre-  
437 industrial atmosphere and the present atmosphere in terms of the ozone generation  
438 environment and the ozone depletion environment.

Furthermore, the *PiClim-2VOC* experiment in the CESM and GFDL models lead to an increase in tropospheric O<sub>3</sub> volume mixing ratio, despite not reproducing higher O<sub>3</sub> chemical production. The UKESM model successfully captures the enhancement of O<sub>3</sub> chemical formation due to increased emissions of VOCs from natural sources, underscoring its precise sensitivity to these emissions and validating its capability to simulate O<sub>3</sub> dynamics influenced by them. However, the global O<sub>3</sub> volume mixing ratio in the *PiClim-2xVOC* experiment of these models is lower than that of the *PiClim-VOC* experiment. These observations illustrate the variability among models in capturing the O<sub>3</sub> response to its precursor species, stemming from varied treatments of critical atmospheric processes, including photolysis, dry deposition, transport mechanisms, and mixing dynamics. Furthermore, these findings highlight the variability in global O<sub>3</sub> sensitivity compared to local O<sub>3</sub> sensitivity, underscoring the complexity of studying O<sub>3</sub> sensitivity on a global scale to mitigate its climate impacts.

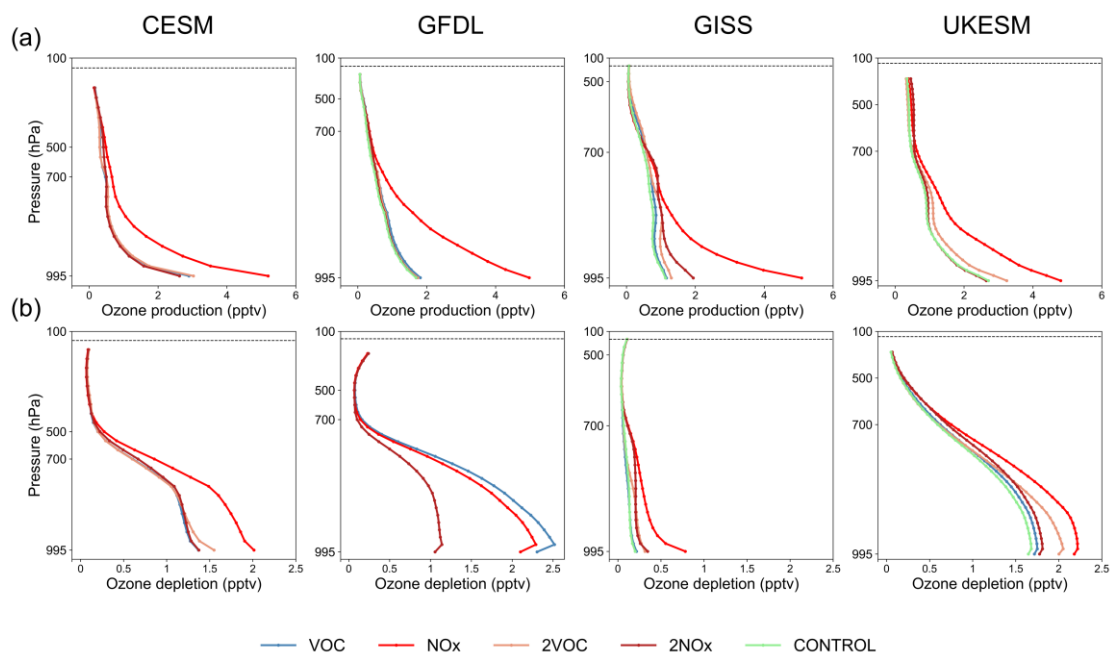
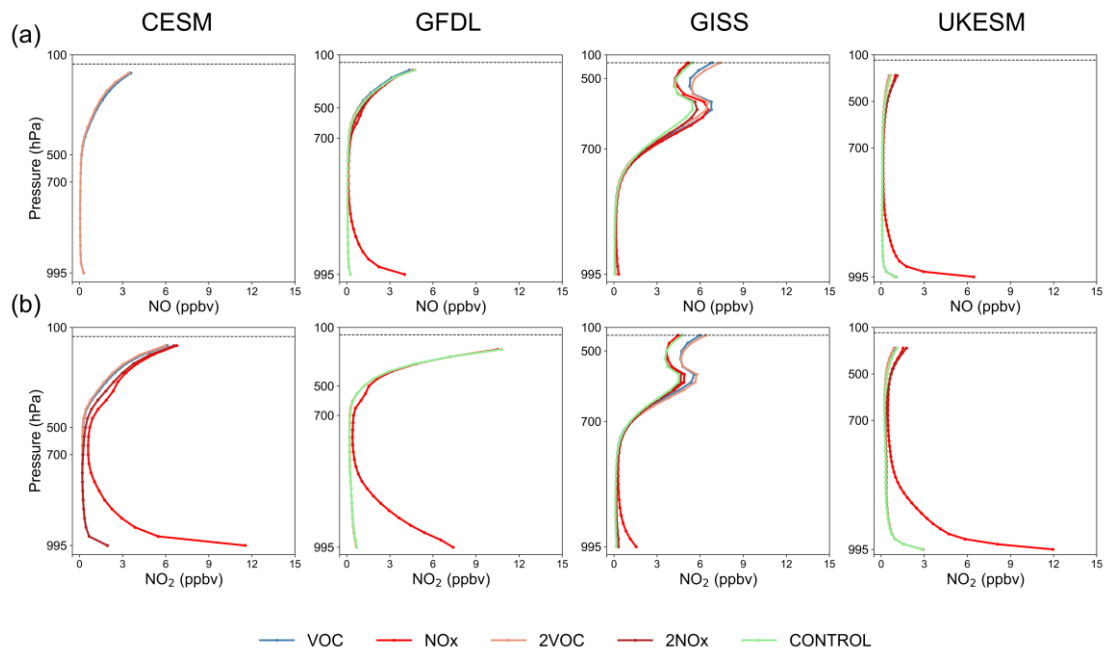


**Figure 4.** Vertical profiles of O<sub>3</sub> volume mixing ratio (a) chemical production and (b) chemical depletion rate for the 30<sup>th</sup> year across five [experiments](#) in the four models.

Figure 4b illustrates that, apart from the O<sub>3</sub> chemical formation mechanism, the CESM, GFDL, and UKESM models in the *PiClim-2NO<sub>x</sub>* experiment do not accurately depict the O<sub>3</sub> chemical depletion process induced by NO<sub>x</sub>. Despite successfully replicating the rise in NO and NO<sub>2</sub> levels (Fig. 5a, b) in the upper troposphere, these models fall short in capturing the NO<sub>x</sub>-related O<sub>3</sub> depletion phenomenon. Moreover, the GISS model stands out with notably elevated NO<sub>x</sub> volume mixing ratios attributed to heightened lightning activity compared to the other

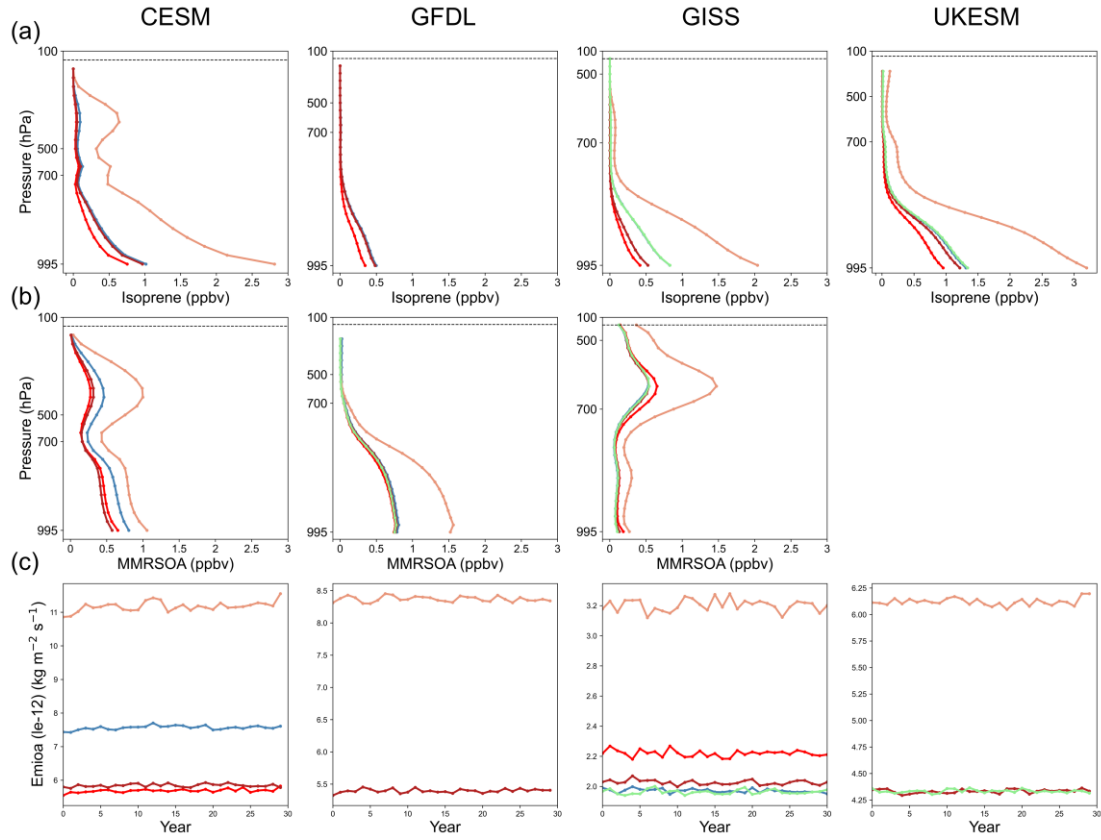
462 models. Additionally, it demonstrates a peak NO<sub>x</sub> volume mixing ratio near 500 hPa  
 463 across [these four](#)<sup>all</sup> experiments conducted, a feature not observed in the other models.



464  
 465 **Figure 5.** Vertical profiles of (a) NO and (b) NO<sub>2</sub> volume mixing ratios for the 30th  
 466 year across five experiments in the four models.

467 Figure 6 illustrates a notable inverse correlation between the consumption of  
 468 isoprene and the chemical production of O<sub>3</sub> in four models, when the rise in VOCs  
 469 emissions is not factored in. This relationship is attributed to the significance of  
 470 isoprene as a natural VOC source in unpolluted atmospheres and highlights the  
 471 absence of O<sub>3</sub> generation simulation due to lightning activity in the CESM, GFDL,  
 472 and UKESM models. In the *PiClim* experiments, the UKESM model did not provide  
 473 mass fraction of secondary particulate organic matter dry aerosol particles in the air  
 474 (mmrsoa), and so we only include its volume mixing ratio of isoprene in the air (isop)  
 475 and the primary emissions and chemical production of dry aerosol organic matter  
 476 (emioa) in Fig. 6. Additionally, the CESM model exhibits higher emissions and  
 477 chemical formation of organic dry aerosol particles compared to the GFDL and GISS  
 478 models. This difference potentially contributes to the observed variation in global O<sub>3</sub>  
 479 volume mixing ratios, with the highest levels recorded in the CESM model and the  
 480 lowest in the GISS model.

481



482  
483 **Figure 6.** Vertical profiles of (a) isoprene volume mixing ratio and (b) secondary  
484 organic aerosol mass mixing ratio for the 30<sup>th</sup> year of all available experiments across  
485 the three models. (c) Temporal evolution characteristics of major emissions and the  
486 chemical production of organic dry aerosol particles from five experiments of the four  
487 models.

#### 488 4. Conclusions

489 This study assessed the sensitivity of global-scale ozone ( $O_3$ ) to precursor gases  
490 in a clean atmosphere and evaluated the simulation capabilities of four Earth system  
491 models using data from the *PiClim* experiments within the AerChemMIP framework.  
492 Our results highlight both strengths and limitations of these models in capturing  $O_3$   
493 dynamicsresponse. The CESM and GFDL models excelled in reproducing seasonal  
494  $O_3$  cycles and the vertical distribution of  $O_3$ , but they showed limitations in simulating  
495 the tropospheric  $O_3$  response to  $NO_x$  emissions from natural sources, such as lightning  
496 activity. Conversely, the GISS and UKESM models effectively simulated the positive  
497 correlation between tropospheric  $O_3$  and temperature but were less sensitive to natural  
498 precursors compared to anthropogenic sources. Discrepancies, such as zonal

499 temperature biases in the GISS model and stratospheric temperature inconsistencies  
500 in the GFDL model, underscore areas for improvement.

501 Our findings suggest that existing assumptions regarding O<sub>3</sub> sensitivity to  
502 natural precursors may require refinement in clean atmospheric conditions. This  
503 research provides critical insights into the interplay between O<sub>3</sub> and its precursors,  
504 enhancing the accuracy of O<sub>3</sub> simulations in Earth system models. Given the  
505 significant role of O<sub>3</sub> in radiative forcing, atmospheric oxidation, and climate  
506 feedback mechanisms, our study reinforces the necessity of precise modeling to better  
507 predict and mitigate future climate scenarios. Additionally, the results underscore the  
508 importance of controlling anthropogenic precursor emissions as an essential strategy  
509 to manage tropospheric O<sub>3</sub> volume mixing ratios and address broader climate change  
510 challenges. Furthermore, among the models analyzed, only the GISS model  
511 demonstrates a significant increase in Antarctic ozone levels compared to the Arctic  
512 (Fig. 3); the other three models yield similar ozone concentrations at both polar  
513 regions. This discrepancy seems to result from a distinct characteristic of the GISS  
514 model's dynamical representation of the Antarctic polar vortex. Figure 1 also reveals  
515 that the ozone difference in the GISS model is predominantly confined to JJA and  
516 SON (Antarctic winter-spring).

517 It is important to acknowledge that the results generated by the models are  
518 accompanied by a degree of uncertainty. Variations in the methodologies employed  
519 by different models to address chemical reactions, including the production and  
520 depletion of ozone, contribute to the uncertainty surrounding the ozone budget.  
521 Furthermore, discrepancies in the data pertaining to anthropogenic and natural  
522 emissions, particularly concerning NO<sub>x</sub> and BVOC emissions, substantially influence  
523 the outcomes of these models. Additionally, the uncertainty associated with the  
524 stratosphere-troposphere exchange process represents a critical factor in the ozone  
525 budget, with notable divergences in the treatment of this process across various  
526 models.

## 527 Acknowledgement

528 We acknowledge the World Climate Research Programme, which, through its  
529 Working Group on Coupled Modelling, coordinated and promoted CMIP6. We thank  
530 the climate modelling groups for producing and making available their model output,

531 the Earth System Grid Federation (ESGF) for archiving the data and providing access,  
532 and the multiple funding agencies who support CMIP6 and ESGF. We acknowledge  
533 the AerChemMIP groups of the four models used in the study (Vaishali Naik and  
534 Larry Horowitz for the GFDL simulations, Susanne E. Bauer and Kostas Tsigaridis  
535 for the GISS simulations, Fiona O'Connor and Jonny Williams for the UKESM  
536 simulations, as well as Louisa K. Emmons for the NCAR simulations). Particularly,  
537 we are grateful to Dr. Vaishali Naik for her comments and suggestions during the  
538 revision of this manuscript. We also thank the editor and anonymous reviewers for  
539 their time and comments, which helped improve the quality of this work greatly.

#### 540 **Data availability**

541 All data from the Earth system models used in this paper are available on the  
542 Earth System Grid Federation website and can be downloaded from <https://esgf-index1.ceda.ac.uk/search/cmip6-ceda/> (last access: 4 July 2024, ESGF-CEDA, 2024).

#### 544 **Author contributions**

545 WW and CYG provided data analysis and contributed to the writing and  
546 discussion of this paper.

#### 547 **Competing interests**

548 The authors declare that they have no conflict of interest.

#### 549 **References**

550 Archibald, A. T., O'Connor, F. M., Abraham, N. L., Archer-Nicholls, S., Chipperfield,  
551 M. P., Dalvi, M., Folberth, G. A., Dennison, F., Dhomse, S. S., Griffiths, P. T.,  
552 Hardacre, C., Hewitt, A. J., Hill, R. S., Johnson, C. E., Keeble, J., Kohler, M. O.,  
553 Morgenstern, O., Mulcahy, J. P., Ordonez, C., Pope, R. J., Rumbold, S. T., Russo, M.  
554 R., Savage, N. H., Sellar, A., Stringer, M., Turnock, S. T., Wild, O., and Zeng, G.:  
555 Description and evaluation of the UKCA stratosphere-troposphere chemistry scheme  
556 (StratTrop vn 1.0) implemented in UKESM1, Geoscientific Model Development, 13,  
557 1223-1266, 10.5194/gmd-13-1223-2020, 2020.

558 Austin, J., Horowitz, L. W., Schwarzkopf, M. D., Wilson, R. J., and Levy, H., II:  
559 Stratospheric ozone and temperature simulated from the preindustrial era to the  
560 present day, Journal of Climate, 26, 3528-3543, 10.1175/jcli-d-12-00162.1, 2013.

561 Bauer, S. E., Tsigaridis, K., Faluvegi, G., Kelley, M., Lo, K. K., Miller, R. L.,  
562 Nazarenko, L., Schmidt, G. A., and Wu, J.: Historical (1850-2014) Aerosol evolution  
563 and role on climate forcing using the GISS ModelE2.1 contribution to CMIP6,  
564 Journal of Advances in Modeling Earth Systems, 12, 10.1029/2019ms001978, 2020.

565 Brown, F., Folberth, G. A., Sitch, S., Bauer, S., Bauters, M., Boeckx, P., Cheesman,  
566 A. W., Deushi, M., Dos Santos, I., Galy-Lacaux, C., Haywood, J., Keeble, J.,  
567 Mercado, L. M., O'Connor, F. M., Oshima, N., Tsigaridis, K., and Verbeeck, H.: The  
568 ozone-climate penalty over South America and Africa by 2100, *Atmospheric  
569 Chemistry and Physics*, 22, 12331-12352, 10.5194/acp-22-12331-2022, 2022.

570 Carrillo-Torres, E. R., Hernandez-Paniagua, I. Y., and Mendoza, A.: Use of combined  
571 observational-and model-derived photochemical indicators to assess the O<sub>3</sub>-NO<sub>x</sub>-  
572 VOC system sensitivity in urban areas, *Atmosphere*, 8, 10.3390/atmos8020022, 2017.

573 Coffman, E., Rappold, A. G., Nethery, R. C., Anderton, J., Amend, M., Jackson, M.  
574 A., Roman, H., Fann, N., Baker, K. R., and Sacks, J. D.: Quantifying multipollutant  
575 health impacts using the environmental benefits mapping and analysis program-  
576 community edition (BenMAP-CE): A case study in Atlanta, Georgia, *Environment  
577 Health Perspect*, 132, 37003, 10.1289/EHP12969, 2024.

578 Collins, W. J., Lamarque, J.-F., Schulz, M., Boucher, O., Eyring, V., Hegglin, M. I.,  
579 Maycock, A., Myhre, G., Prather, M., Shindell, D., and Smith, S. J.: AerChemMIP:  
580 quantifying the effects of chemistry and aerosols in CMIP6, *Geoscientific Model  
581 Development*, 10, 585-607, 10.5194/gmd-10-585-2017, 2017.

582 Dunne, J. P., Horowitz, L. W., Adcroft, A. J., Ginoux, P., Held, I. M., John, J. G.,  
583 Krasting, J. P., Malyshev, S., Naik, V., Paulot, F., Shevliakova, E., Stock, C. A.,  
584 Zadeh, N., Balaji, V., Blanton, C., Dunne, K. A., Dupuis, C., Durachta, J., Dussin, R.,  
585 Gauthier, P. P. G., Griffies, S. M., Guo, H., Hallberg, R. W., Harrison, M., He, J.,  
586 Hurlin, W., McHugh, C., Menzel, R., Milly, P. C. D., Nikonorov, S., Paynter, D. J.,  
587 Poshay, J., Radhakrishnan, A., Rand, K., Reichl, B. G., Robinson, T., Schwarzkopf,  
588 D. M., Sentman, L. T., Underwood, S., Vahlenkamp, H., Winton, M., Wittenberg, A.  
589 T., Wyman, B., Zeng, Y., and Zhao, M.: The GFDL earth system model version 4.1  
590 (GFDL-ESM 4.1): Overall coupled model description and simulation characteristics,  
591 *Journal of Advances in Modeling Earth Systems*, 12, 10.1029/2019ms002015, 2020.

592 Fowler, D., Pilegaard, K., Sutton, M. A., Ambus, P., Raivonen, M., Duyzer, J.,  
593 Simpson, D., Fagerli, H., Fuzzi, S., Schjoerring, J. K., Granier, C., Neftel, A., Isaksen,  
594 I. S. A., Laj, P., Maione, M., Monks, P. S., Burkhardt, J., Daemmggen, U., Neirynck,  
595 J., Personne, E., Wichink-Kruit, R., Butterbach-Bahl, K., Flechard, C., Tuovinen, J.  
596 P., Coyle, M., Gerosa, G., Loubet, B., Altimir, N., Gruenhage, L., Ammann, C.,  
597 Cieslik, S., Paoletti, E., Mikkelsen, T. N., Ro-Poulsen, H., Cellier, P., Cape, J. N.,  
598 Horvath, L., Loreto, F., Niinemets, U., Palmer, P. I., Rinne, J., Misztal, P., Nemitz,  
599 E., Nilsson, D., Pryor, S., Gallagher, M. W., Vesala, T., Skiba, U., Brueggemann, N.,  
600 Zechmeister-Boltenstern, S., Williams, J., O'Dowd, C., Facchini, M. C., de Leeuw,  
601 G., Flossman, A., Chaumerliac, N., and Erisman, J. W.: Atmospheric composition  
602 change: Ecosystems-atmosphere interactions, *Atmospheric Environment*, 43, 5193-  
603 5267, 10.1016/j.atmosenv.2009.07.068, 2009.

604 Gettelman, A., Hannay, C., Bacmeister, J. T., Neale, R. B., Pendergrass, A. G.,  
605 Danabasoglu, G., Lamarque, J. F., Fasullo, J. T., Bailey, D. A., Lawrence, D. M., and  
606 Mills, M. J.: High climate sensitivity in the Community Earth System Model Version  
607 2 (CESM2), *Geophysical Research Letters*, 46, 8329-8337, 10.1029/2019gl083978,  
608 2019.

609 Griffiths, P. T., Murray, L. T., Zeng, G., Shin, Y. M., Abraham, N. L., Archibald, A.  
610 T., Deushi, M., Emmons, L. K., Galbally, I. E., Hassler, B., Horowitz, L. W., Keeble,

611 J., Liu, J., Moeini, O., Naik, V., O'Connor, F. M., Oshima, N., Tarasick, D., Tilmes,  
612 S., Turnock, S. T., Wild, O., Young, P. J., and Zanis, P.: Tropospheric ozone in  
613 CMIP6 simulations, *Atmospheric Chemistry and Physics*, 21, 4187-4218,  
614 10.5194/acp-21-4187-2021, 2021.

615 Guenther, A., Hewitt, C. N., Erickson, D., Fall, R., Geron, C., Graedel, T., Harley, P.,  
616 Klinger, L., Lerdau, M., Mckay, W. A., Pierce, T., Scholes, B., Steinbrecher, R.,  
617 Tallamraju, R., Taylor, J., and Zimmerman, P.: A global model of natural volatile  
618 organic compound emissions, *Journal of Geophysical Research-Atmospheres*, 100,  
619 8873-8892, <https://doi.org/10.1029/94JD02950>, 1995.

620 Guenther, A. B., Jiang, X., Heald, C. L., Sakulyanontvittaya, T., Duhl, T., Emmons,  
621 L. K., and Wang, X.: The Model of Emissions of Gases and Aerosols from Nature  
622 version 2.1 (MEGAN2.1): an extended and updated framework for modeling biogenic  
623 emissions, *Geoscientific Model Development*, 5, 1471-1492, 10.5194/gmd-5-1471-  
624 2012, 2012.

625 Hakim, Z. Q., Archer-Nicholls, S., Beig, G., Folberth, G. A., Sudo, K., Abraham, N.  
626 L., Ghude, S., Henze, D. K., and Archibald, A. T.: Evaluation of tropospheric ozone  
627 and ozone precursors in simulations from the HTAPII and CCMI model  
628 intercomparisons — a focus on the Indian subcontinent, *Atmospheric Chemistry and  
629 Physics*, 19, 6437-6458, 10.5194/acp-19-6437-2019, 2019.

630 Horowitz, L. W., Naik, V., Paulot, F., Ginoux, P. A., Dunne, J. P., Mao, J., Schnell,  
631 J., Chen, X., He, J., John, J. G., Lin, M., Lin, P., Malyshev, S., Paynter, D.,  
632 Shevliakova, E., and Zhao, M.: The GFDL global atmospheric chemistry-climate  
633 model AM4.1: Model description and simulation characteristics, *Journal of Advances  
634 in Modeling Earth Systems*, 12, 10.1029/2019ms002032, 2020.

635 Hu, L., Wang, Z., Huang, M., Sun, H., and Wang, Q.: A remote sensing based method  
636 for assessing the impact of O<sub>3</sub> on the net primary productivity of terrestrial  
637 ecosystems in China, *Frontiers in Environmental Science*, 11,  
638 10.3389/fenvs.2023.1112874, 2023.

639 Jin, X., Fiore, A. M., and Cohen, R. C.: Space-based observations of ozone precursors  
640 within California wildfire plumes and the impacts on ozone-NO<sub>x</sub>-VOC chemistry,  
641 *Environmental Science & Technology*, 57, 14648-14660, 10.1021/acs.est.3c04411,  
642 2023.

643 Karl, T., Lamprecht, C., Graus, M., Cede, A., Tiefengraber, M., de Arellano, J. V. -  
644 G., Gurarie, D., and Lenschow, D.: High urban NO<sub>x</sub> triggers a substantial chemical  
645 downward flux of ozone, *Science Advances*, 9, 10.1126/sciadv.add2365, 2023.

646 Karset, I. H. H., Berntsen, T. K., Storelvmo, T., Alterskjaer, K., Grini, A., Olivie, D.,  
647 Kirkevag, A., Seland, O., Iversen, T., and Schulz, M.: Strong impacts on aerosol  
648 indirect effects from historical oxidant changes, *Atmospheric Chemistry and Physics*,  
649 18, 7669-7690, 10.5194/acp-18-7669-2018, 2018.

650 Kelley, M., Schmidt, G. A., Nazarenko, L. S., Bauer, S. E., Ruedy, R., Russell, G. L.,  
651 Ackerman, A. S., Aleinov, I., Bauer, M., Bleck, R., Canuto, V., Cesana, G., Cheng,  
652 Y., Clune, T. L., Cook, B. I., Cruz, C. A., Del Genio, A. D., Elsaesser, G. S., Faluvegi,  
653 G., Kiang, N. Y., Kim, D., Lacis, A. A., Leboissetier, A., LeGrande, A. N., Lo, K. K.,  
654 Marshall, J., Matthews, E. E., McDermid, S., Mezuman, K., Miller, R. L., Murray, L.  
655 T., Oinas, V., Orbe, C., Perez Garcia-Pando, C., Perlitz, J. P., Puma, M. J., Rind,

656 D., Romanou, A., Shindell, D. T., Sun, S., Tausnev, N., Tsigaridis, K., Tselioudis, G.,  
657 Weng, E., Wu, J., and Yao, M.-S.: GISS-E2.1: Configurations and climatology,  
658 Journal of Advances in Modeling Earth Systems, 12, 10.1029/2019ms002025, 2020.

659 Khomsi, K., Chelhaoui, Y., Alilou, S., Souri, R., Najmi, H., and Souhaili, Z.:  
660 Concurrent heat waves and extreme ozone ( $O_3$ ) episodes: Combined atmospheric  
661 patterns and impact on human health, International Journal of Environmental  
662 Research and Public Health, 19, 10.3390/ijerph19052770, 2022.

663 Kumaş, K., Akyüz, A. J. I. J. o. E., and Geoinformatics: Estimation of greenhouse  
664 gas emission and global warming potential of livestock sector; Lake District, Türkiye,  
665 2023.

666 Li, M., Huang, X., Yan, D., Lai, S., Zhang, Z., Zhu, L., Lu, Y., Jiang, X., Wang, N.,  
667 Wang, T., Song, Y., and Ding, A.: Coping with the concurrent heatwaves and ozone  
668 extremes in China under a warming climate, Science Bulletin, 69, 2938-2947,  
669 <https://doi.org/10.1016/j.scib.2024.05.034>, 2024.

670 Lim, C. C., Hayes, R. B., Ahn, J., Shao, Y., Silverman, D. T., Jones, R. R., Garcia,  
671 C., Bell, M. L., and Thurston, G. D.: Long-term exposure to ozone and cause-specific  
672 mortality risk in the United States, American Journal of Respiratory and Critical Care  
673 Medicine, 200, 1022-1031, 10.1164/rccm.201806-1161OC, 2019.

674 Malley, C. S., Henze, D. K., Kuylenstierna, J. C. I., Vallack, H. W., Davila, Y.,  
675 Anenberg, S. C., Turner, M. C., and Ashmore, M. R.: Updated global estimates of  
676 respiratory mortality in adults  $\geq 30$  years of age attributable to long-term ozone  
677 exposure, Environment Health Perspect, 125, 087021, 10.1289/EHP1390, 2017.

678 Miller, R. L., Schmidt, G. A., Nazarenko, L. S., Tausnev, N., Bauer, S. E., DelGenio,  
679 A. D., Kelley, M., Lo, K. K., Ruedy, R., Shindell, D. T., Aleinov, I., Bauer, M., Bleck,  
680 R., Canuto, V., Chen, Y., Cheng, Y., Clune, T. L., Faluvegi, G., Hansen, J. E., Healy,  
681 R. J., Kiang, N. Y., Koch, D., Lacis, A. A., LeGrande, A. N., Lerner, J., Menon, S.,  
682 Oinas, V., Garcia-Pando, C. P., Perlitz, J. P., Puma, M. J., Rind, D., Romanou, A.,  
683 Russell, G. L., Sato, M., Sun, S., Tsigaridis, K., Unger, N., Voulgarakis, A., Yao, M.-  
684 S., and Zhang, J.: CMIP5 historical simulations (1850-2012) with GISS ModelE2,  
685 Journal of Advances in Modeling Earth Systems, 6, 441-477, 10.1002/2013ms000266,  
686 2014.

687 Möller, D. and Mauersberger, G.: Cloud chemistry effects on tropospheric  
688 photooxidants in polluted atmosphere — Model results, Journal of Atmospheric  
689 Chemistry, 14, 153-165, 10.1007/BF00115231, 1992.

690 Monks, P. S., Archibald, A. T., Colette, A., Cooper, O., Coyle, M., Derwent, R.,  
691 Fowler, D., Granier, C., Law, K. S., Mills, G. E., Stevenson, D. S., Tarasova, O.,  
692 Thouret, V., von Schneidemesser, E., Sommariva, R., Wild, O., and Williams, M. L.:  
693 Tropospheric ozone and its precursors from the urban to the global scale from air  
694 quality to short-lived climate forcer, Atmospheric Chemistry and Physics, 15, 8889-  
695 8973, 10.5194/acp-15-8889-2015, 2015.

696 Mulcahy, J. P., Jones, C., Sellar, A., Johnson, B., Boutle, I. A., Jones, A., Andrews,  
697 T., Rumbold, S. T., Molland, J., Bellouin, N., Johnson, C. E., Williams, K. D.,  
698 Grosvenor, D. P., and McCoy, D. T.: Improved aerosol processes and effective  
699 radiative forcing in HadGEM3 and UKESM1, Journal of Advances in Modeling Earth  
700 Systems, 10, 2786-2805, 10.1029/2018ms001464, 2018.

701 Murray, L. T., Logan, J. A., and Jacob, D. J.: Interannual variability in tropical  
702 tropospheric ozone and OH: The role of lightning, *Journal of Geophysical Research-Atmospheres*, 118, 11,468-411,480, <https://doi.org/10.1002/jgrd.50857>, 2013.

703

704 Naik, V., Horowitz, L. W., Fiore, A. M., Ginoux, P., Mao, J., Aghedo, A. M., and  
705 Levy, H., II: Impact of preindustrial to present-day changes in short-lived pollutant  
706 emissions on atmospheric composition and climate forcing, *Journal of Geophysical  
707 Research-Atmospheres*, 118, 8086-8110, 10.1002/jgrd.50608, 2013a.

708 Naik, V., Voulgarakis, A., Fiore, A. M., Horowitz, L. W., Lamarque, J. F., Lin, M.,  
709 Prather, M. J., Young, P. J., Bergmann, D., Cameron-Smith, P. J., Cionni, I., Collins,  
710 W. J., Dalsøren, S. B., Doherty, R., Eyring, V., Faluvegi, G., Folberth, G. A., Josse,  
711 B., Lee, Y. H., MacKenzie, I. A., Nagashima, T., van Noije, T. P. C., Plummer, D.  
712 A., Righi, M., Rumbold, S. T., Skeie, R., Shindell, D. T., Stevenson, D. S., Strode,  
713 S., Sudo, K., Szopa, S., and Zeng, G.: Preindustrial to present-day changes in  
714 tropospheric hydroxyl radical and methane lifetime from the Atmospheric Chemistry  
715 and Climate Model Intercomparison Project (ACCMIP), *Atmospheric Chemistry and  
716 Physics*, 13, 5277-5298, 10.5194/acp-13-5277-2013, 2013b.

717 Nuvolone, D., Petri, D., and Voller, F.: The effects of ozone on human health,  
718 *Environmental Science and Pollution Research*, 25, 8074-8088, 10.1007/s11356-017-  
719 9239-3, 2018.

720 Pacifico, F., Harrison, S. P., Jones, C. D., Arneth, A., Sitch, S., Weedon, G. P.,  
721 Barkley, M. P., Palmer, P. I., Serca, D., Potosnak, M., Fu, T. M., Goldstein, A., Bai,  
722 J., and Schurgers, G.: Evaluation of a photosynthesis-based biogenic isoprene  
723 emission scheme in JULES and simulation of isoprene emissions under present-day  
724 climate conditions, *Atmospheric Chemistry and Physics*, 11, 4371-4389,  
725 10.5194/acp-11-4371-2011, 2011.

726 Price, C. and Rind, D.: A simple lightning parameterization for calculating global  
727 lightning distributions, *Journal of Geophysical Research-Atmospheres*, 97, 9919-  
728 9933, <https://doi.org/10.1029/92JD00719>, 1992.

729 Price, C., Penner, J., and Prather, M.: NO<sub>x</sub> from lightning: 1. Global distribution based  
730 on lightning physics, *Journal of Geophysical Research-Atmospheres*, 102, 5929-5941,  
731 <https://doi.org/10.1029/96JD03504>, 1997.

732 Price, C. G.: Lightning applications in weather and climate research, *Surveys in  
733 Geophysics*, 34, 755-767, 10.1007/s10712-012-9218-7, 2013.

734 Rogelj, J., Schaeffer, M., Meinshausen, M., Shindell, D. T., Hare, W., Klimont, Z.,  
735 Velders, G. J. M., Amann, M., and Schellnhuber, H. J.: Disentangling the effects of  
736 CO<sub>2</sub> and short-lived climate forcer mitigation, *Proceedings of the National Academy  
737 of Sciences of the United States of America*, 111, 16325-16330,  
738 10.1073/pnas.1415631111, 2014.

739 Romanowsky, E., Handorf, D., Jaiser, R., Wohltmann, I., Dorn, W., Ukita, J., Cohen,  
740 J., Dethloff, K., and Rex, M.: The role of stratospheric ozone for Arctic-midlatitude  
741 linkages, *Scientific Reports*, 9, 7962, 10.1038/s41598-019-43823-1, 2019.

742 Schnell, J. L., Naik, V., Horowitz, L. W., Paulot, F., Mao, J., Ginoux, P., Zhao, M.,  
743 and Ram, K.: Exploring the relationship between surface PM<sub>2.5</sub> and meteorology in

744 Northern India, *Atmospheric Chemistry and Physics*, 18, 10157-10175, 10.5194/acp-  
745 18-10157-2018, 2018.

746 Sellar, A. A., Jones, C. G., Mulcahy, J. P., Tang, Y., Yool, A., Wiltshire, A., O'Connor,  
747 F. M., Stringer, M., Hill, R., Palmieri, J., Woodward, S., de Mora, L., Kuhlbrodt, T.,  
748 Rumbold, S. T., Kelley, D. I., Ellis, R., Johnson, C. E., Walton, J., Abraham, N. L.,  
749 Andrews, M. B., Andrews, T., Archibald, A. T., Berthou, S., Burke, E., Blockley, E.,  
750 Carslaw, K., Dalvi, M., Edwards, J., Folberth, G. A., Gedney, N., Griffiths, P. T.,  
751 Harper, A. B., Hendry, M. A., Hewitt, A. J., Johnson, B., Jones, A., Jones, C. D.,  
752 Keeble, J., Liddicoat, S., Morgenstern, O., Parker, R. J., Predoi, V., Robertson, E.,  
753 Siahaan, A., Smith, R. S., Swaminathan, R., Woodhouse, M. T., Zeng, G., and  
754 Zerroukat, M.: UKESM1: Description and evaluation of the UK earth system model,  
755 *Journal of Advances in Modeling Earth Systems*, 11, 4513-4558,  
756 10.1029/2019ms001739, 2019.

757 Shindell, D. T., Faluvegi, G., Unger, N., Aguilar, E., Schmidt, G. A., Koch, D. M.,  
758 Bauer, S. E., and Miller, R. L.: Simulations of preindustrial, present-day, and 2100  
759 conditions in the NASA GISS composition and climate model G-PUCCINI,  
760 *Atmospheric Chemistry and Physics*, 6, 4427-4459, 10.5194/acp-6-4427-2006, 2006.

761 Shindell, D. T., Pechony, O., Voulgarakis, A., Faluvegi, G., Nazarenko, L., Lamarque,  
762 J. F., Bowman, K., Milly, G., Kovari, B., Ruedy, R., and Schmidt, G. A.: Interactive  
763 ozone and methane chemistry in GISS-E2 historical and future climate simulations,  
764 *Atmospheric Chemistry and Physics*, 13, 2653-2689, 10.5194/acp-13-2653-2013,  
765 2013.

766 Sillman, S. and He, D.: Some theoretical results concerning O<sub>3</sub>-NO<sub>x</sub>-VOC chemistry  
767 and NO<sub>x</sub>-VOC indicators, *Journal of Geophysical Research-Atmospheres*, 107, ACH  
768 26-21-ACH 26-15, <https://doi.org/10.1029/2001JD001123>, 2002.

769 Sporre, M. K., Blichner, S. M., Karset, I. H. H., Makkonen, R., and Berntsen, T. K.:  
770 BVOC-aerosol-climate feedbacks investigated using NorESM, *Atmospheric  
771 Chemistry and Physics*, 19, 4763-4782, 10.5194/acp-19-4763-2019, 2019.

772 Stevenson, D. S., Young, P. J., Naik, V., Lamarque, J. F., Shindell, D. T., Voulgarakis,  
773 A., Skeie, R. B., Dalsoren, S. B., Myhre, G., Berntsen, T. K., Folberth, G. A.,  
774 Rumbold, S. T., Collins, W. J., MacKenzie, I. A., Doherty, R. M., Zeng, G., van Noije,  
775 T. P. C., Strunk, A., Bergmann, D., Cameron-Smith, P., Plummer, D. A., Strode, S.  
776 A., Horowitz, L., Lee, Y. H., Szopa, S., Sudo, K., Nagashima, T., Josse, B., Cionni,  
777 I., Righi, M., Eyring, V., Conley, A., Bowman, K. W., Wild, O., and Archibald, A.:  
778 Tropospheric ozone changes, radiative forcing and attribution to emissions in the  
779 Atmospheric Chemistry and Climate Model Intercomparison Project (ACCMIP),  
780 *Atmospheric Chemistry and Physics*, 13, 3063-3085, 10.5194/acp-13-3063-2013,  
781 2013.

782 Stevenson, D. S., Dentener, F. J., Schultz, M. G., Ellingsen, K., van Noije, T. P. C.,  
783 Wild, O., Zeng, G., Amann, M., Atherton, C. S., Bell, N., Bergmann, D. J., Bey, I.,  
784 Butler, T., Cofala, J., Collins, W. J., Derwent, R. G., Doherty, R. M., Drevet, J., Eskes,  
785 H. J., Fiore, A. M., Gauss, M., Hauglustaine, D. A., Horowitz, L. W., Isaksen, I. S.  
786 A., Krol, M. C., Lamarque, J. F., Lawrence, M. G., Montanaro, V., Müller, J. F., Pitari,  
787 G., Prather, M. J., Pyle, J. A., Rast, S., Rodriguez, J. M., Sanderson, M. G., Savage,  
788 N. H., Shindell, D. T., Strahan, S. E., Sudo, K., and Szopa, S.: Multimodel ensemble

789 simulations of present-day and near-future tropospheric ozone, *Journal of*  
790 *Geophysical Research-Atmospheres*, 111, 10.1029/2005jd006338, 2006.

791 Tilmes, S., Visioni, D., Jones, A., Haywood, J., Seferian, R., Nabat, P., Boucher, O.,  
792 Bednarz, E. M., and Niemeier, U.: Stratospheric ozone response to sulfate aerosol  
793 and solar dimming climate interventions based on the G6 Geoengineering Model  
794 Intercomparison Project (GeoMIP) simulations, *Atmospheric Chemistry and Physics*,  
795 22, 4557-4579, 10.5194/acp-22-4557-2022, 2022.

796 Unger, N.: On the role of plant volatiles in anthropogenic global climate change,  
797 *Geophysical Research Letters*, 41, 8563-8569,  
798 <https://doi.org/10.1002/2014GL061616>, 2014.

799 van Marle, M. J. E., Kloster, S., Magi, B. I., Marlon, J. R., Daniau, A. L., Field, R.  
800 D., Arneth, A., Forrest, M., Hantson, S., Kehrwald, N. M., Knorr, W., Lasslop, G.,  
801 Li, F., Mangeon, S., Yue, C., Kaiser, J. W., and van der Werf, G. R.: Historic global  
802 biomass burning emissions for CMIP6 (BB4CMIP) based on merging satellite  
803 observations with proxies and fire models (1750–2015), *Geoscientific Model  
804 Development*, 10, 3329-3357, 10.5194/gmd-10-3329-2017, 2017.

805 Vermeuel, M. P., Novak, G. A., Alwe, H. D., Hughes, D. D., Kaleel, R. J., Dickens,  
806 A., Kenski, D., Czarnetzki, A. C., Stone, E. A., Stanier, C. O., Pierce, R. B., Millet,  
807 D. B., and Bertram, T. H. J. J. o. G. R. A.: Sensitivity of ozone production to NO<sub>x</sub>  
808 and VOC along the lake michigan coastline, *Journal of Geophysical Research-  
809 Atmospheres*, 124, 10989 - 11006, 2019.

810 Walters, D., Baran, A. J., Boutle, I., Brooks, M., Earnshaw, P., Edwards, J., Furtado,  
811 K., Hi, P., Lock, A., Manners, J., Morcrette, C., Mulcahy, J., Sanchez, C., Smith, C.,  
812 Stratton, R., Tennant, W., Tomassini, L., Van Weverberg, K., Vosper, S., Willett, M.,  
813 Browse, J., Bushell, A., Carslaw, K., Dalvi, M., Essery, R., Gedney, N., Hardiman,  
814 S., Johnson, B., Johnson, C., Jones, A., Jones, C., Mann, G., Milton, S., Rumbold, H.,  
815 Sellar, A., Ujiie, M., Whitall, M., Williams, K., and Zerroukat, M.: The met office  
816 unified model global atmosphere 7.0/7.1 and JULES global land 7.0 configurations,  
817 *Geoscientific Model Development*, 12, 1909-1963, 10.5194/gmd-12-1909-2019,  
818 2019.

819 Williams, K. D., Copsey, D., Blockley, E. W., Bodas-Salcedo, A., Calvert, D., Comer,  
820 R., Davis, P., Graham, T., Hewitt, H. T., Hill, R., Hyder, P., Ineson, S., Johns, T. C.,  
821 Keen, A. B., Lee, R. W., Megann, A., Milton, S. F., Rae, J. G. L., Roberts, M. J.,  
822 Scaife, A. A., Schiemann, R., Storkey, D., Thorpe, L., Watterson, I. G., Walters, D.  
823 N., West, A., Wood, R. A., Woollings, T., and Xavier, P. K.: The met office global  
824 coupled model 3.0 and 3.1 (GC3.0 and GC3.1) configurations, *Journal of Advances  
825 in Modeling Earth Systems*, 10, 357-380, 10.1002/2017ms001115, 2018.

826 Young, P. J., Naik, V., Fiore, A. M., Gaudel, A., Guo, J., Lin, M. Y., Neu, J. L.,  
827 Parrish, D. D., Rieder, H. E., Schnell, J. L., Tilmes, S., Wild, O., Zhang, L., Ziemke,  
828 J., Brandt, J., Delcloo, A., Doherty, R. M., Geels, C., Hegglin, M. I., Hu, L., Im, U.,  
829 Kumar, R., Luhar, A., Murray, L., Plummer, D., Rodriguez, J., Saiz-Lopez, A.,  
830 Schultz, M. G., Woodhouse, M. T., and Zeng, G.: Tropospheric ozone assessment  
831 report: assessment of global-scale model performance for global and regional ozone  
832 distributions, variability, and trends, *Elementa-Science of the Anthropocene*, 6,  
833 10.1525/elementa.265, 2018.

834 Zeng, G., Morgenstern, O., Williams, J. H. T., O'Connor, F. M., Griffiths, P. T.,  
835 Keeble, J., Deushi, M., Horowitz, L. W., Naik, V., Emmons, L. K., Abraham, N. L.,  
836 Archibald, A. T., Bauer, S. E., Hassler, B., Michou, M., Mills, M. J., Murray, L. T.,  
837 Oshima, N., Sentman, L. T., Tilmes, S., Tsigaridis, K., and Young, P. J.: Attribution  
838 of stratospheric and tropospheric ozone changes between 1850 and 2014 in CMIP6  
839 models, *Journal of Geophysical Research-Atmospheres*, 127, 10.1029/2022jd036452,  
840 2022.

841